Proc. Lunar Planet. Sci. Conf. 10th (1979), p. 1649–1663.
Printed in the United States of America

Properties of microcraters and cosmic dust of less than 1000 Å dimensions

D. A. Morrison and U. S. Clanton

SN6/NASA Johnson Space Center, Houston, Texas 77058

Abstract—Microcraters from about 100–200 Å to >1000 Å true diameter have been measured by SEM at magnifications of 100,000x on lunar samples 76015,24,9003 and 76015,28,9004. The cumulative size frequency distribution has a slope of ≈–2.5 for craters ≥1000 Å, ≈–1.3 between 1000 Å and 400 Å diameters, and approaches zero at the smallest diameters. Distributions from lunar soil grains exposed during ancient epochs have the same form. Ninety-six of ninety-seven craters observed are equidimensional, indicating equidimensional dust particles with masses as low as 10^{-20} grams. No lower limit on cosmic dust grain sizes was established. The flux and the crater production rate derived are consistent with 12054 measurements.

INTRODUCTION

The properties of microcraters and microcrater populations on lunar sample surfaces and implications thereof concerning the cosmic dust complex have been investigated for a decade (cf. Hörz *et al.*, 1975; Morrison and Zinner, 1977; Hartung *et al.*, 1978), and the microcrater size frequency distribution and production rate on the moon have been characterized reasonably well over the diameter interval 0.1 to several thousand microns. At crater diameters of less than 1000 Å, the results have not been as complete, although the data of Poupeau *et al.* (1975) indicated that such craters and corresponding dust particles occur.

In this paper, we present results of observations of crater populations of 1000 Å and less in diameter which have been made possible by the availability of two unique samples and the development of new sample preparation and scanning electron microscope techniques. The measurement of microcraters hundreds of angstroms or less in size requires magnifications of at least 100,000 times. The latter, in turn, requires coating techniques which eliminate sample charging without obscuring the features to be observed. This capability has only recently been developed. We have applied the new method in the study of two samples which were studied previously by Morrison and Zinner (1975) and known to have substantial microcrater populations.

SAMPLE DESCRIPTION

Sample selection is important in attempting to define the size distribution of microcraters smaller than 1000 Å diameter. The samples examined must have been exposed long enough to have a significant number of craters on mm scale surfaces but simultaneously not have a patina (Blanford *et al.*, 1974) which obscures the microcrater population. The effects of solar wind erosion (McDonnell, 1977) must also be taken into account, which requires a detailed knowledge of exposure geometry.

We have selected two samples which satisfy these criteria. The samples are 76015,24,9003 and 76015,28,9004, which are splits of samples 76015,24 and 28, described by Blanford *et al.* (1974) and Morrison and Zinner (1975 and 1977). These samples had unusual exposure geometries as shown in Fig. 1 taken from Morrison and Zinner (1975). Sample 76015,24,9003 was removed from the bottom or end of the cavity shown in Fig. 1. Blanford *et al.* (1974) estimated the solid angle for this area to be about 0.29 steradians. The long axis of the cavity pointed toward lunar north and surfaces within the cavity were never exposed to solar wind. Sample 76015,28,9004 was exposed over a larger solid angle in the bottom of a cleft as shown in Fig. 1. This solid angle was estimated to be 0.54 steradians (Morrison and Zinner, 1975) but this measurement applied to ,28 and probably represents an upper limit for 76015,28,9004. The exposure was confined to the plane of the ecliptic (Blanford *et al.*, 1974; Morrison and Zinner, 1975). With a solid angle of 0.54 steradians and the orientation of the cavity shown in Fig. 1, it is possible that 76015,28,9004 was exposed to the solar wind. Effective exposure would be about 1/18 of a lunar rotation (i.e., 20°/360°).

The exposure ages of both surfaces are the same as exposure ages of other

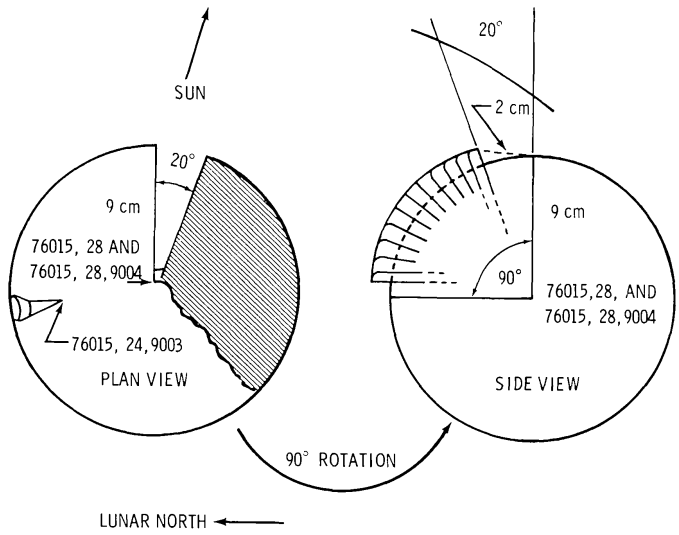

Fig. 1. Reconstruction of the exposure geometry of 76015,28,9004 and 76015,24,9003 and their parents from Morrison and Zinner (1975).

surfaces in the cavities in which they occur because all surfaces in each cavity were exposed simultaneously. Using the Blanford *et al.* (1975) track production model and solar flare track data of Morrison and Zinner (1975), the exposure age of 76015,40 was calculated to be 5.3×10^5 years. This exposure age can also be applied to 76015,24,9003. Similarly, Morrison and Zinner (1975) calculated the exposure age for 76015,105 to be 4.6×10^5 years, which can be applied to 76015,28,9004.

EXPERIMENTAL PROCEDURES

We examined the samples with a JEOL JEM-100C TEMSCAN (Transmission and scanning electron microscope), which is capable of better than 30 Å resolution point-to-point in the SEM mode. As is the case for most microscopes of this type, the sample size is limited to about $1 \times 2 \times 6$ mm.

The earlier work on the parents of both samples included scanning electron microscopy and the samples had been coated with gold. A preliminary examination showed that the coatings had degraded and this gold coating was removed with a KI solution. A solution saturated in KI was prepared and then this solution was saturated with iodine. The coated samples were washed in this solution at room temperature. Several minutes are generally required to remove gold coatings using this technique. The samples were then washed in methanol several times, both at room temperature and at 95°C in a Teflon bomb to remove the KI from the sample. Washing with methanol must be thorough if the samples are porous.

Following the removal of the preexisting gold coat, the samples were recoated with a gold-palladium alloy following a procedure devised by Clanton (1979, pers. comm.). Because this technique may be of some use to others we will describe it in detail.

The typical sample used in SEM analysis requires a conductive coating to prevent a charge buildup under the incident electron beam. Although most workers include some comment as to the type of coating used, only rarely is some coating thickness given in reporting SEM data. Because of the ease of application, availability and excellent secondary electron emission properties, gold is perhaps the most commonly used material. At magnifications of less than 10,000x and with resolutions of 200 to 300 Å, artifacts produced by gold-coating procedures may not be noticed, but as magnification increases to 20,000x and resolution approaches 100 Å, coating artifacts may become the dominant elements in micrographs.

A series of experiments were carried out to develop coatings suitable for very high resolution. The sputtering equipment utilized in the study was a Hummer I manufactured by Technics. The power transformer was replaced for higher voltage (2 KV) and the argon metering system modified for better control than is possible with the original design. The target to sample distance was maintained

throughout the tests at 2.5 cm, the potential was 1600 volts, the current was 10 mA and the pressure was 110 millitorr. The equipment configuration listed above remained unchanged, but the coating time was varied to produce coatings of different thicknesses. The samples and standards for comparison consisted of latex spheres 0.481, 0.312 and 0.109 μm in diameter. Droplets of water containing the dispersed latex spheres were deposited on spectrographic grade carbon planchettes and evaporated to dryness.

The initial efforts were directed toward producing a gold sputtered surface without artifact. Samples were coated with gold with coating time increased in 5 second increments ending with a one minute application. Runs of 3 minutes of sputtering were also used. Figure 2 illustrates the artifact morphology after 40 seconds of gold sputtering. Islands of gold ranging in size from about 50 to 200 Å dominate the surface detail; a few cracks up to about 100 Å wide remain between the islands of gold. After three minutes of gold sputtering, a "blackberry" surface is produced whereby both latex sphere and carbon substrate have been covered by islands of gold some 200 to 300 Å in diameter (Fig. 3).

Gold coated samples obtained from other laboratories (some using sputtering techniques and some using vacuum evaporation techniques) showed similar artifacts. All of the gold coated samples that have been studied from our own and other laboratories have shown coating artifacts. The thickness of the gold coating on the sample appears to be responsible for the type of artifact seen. Because we

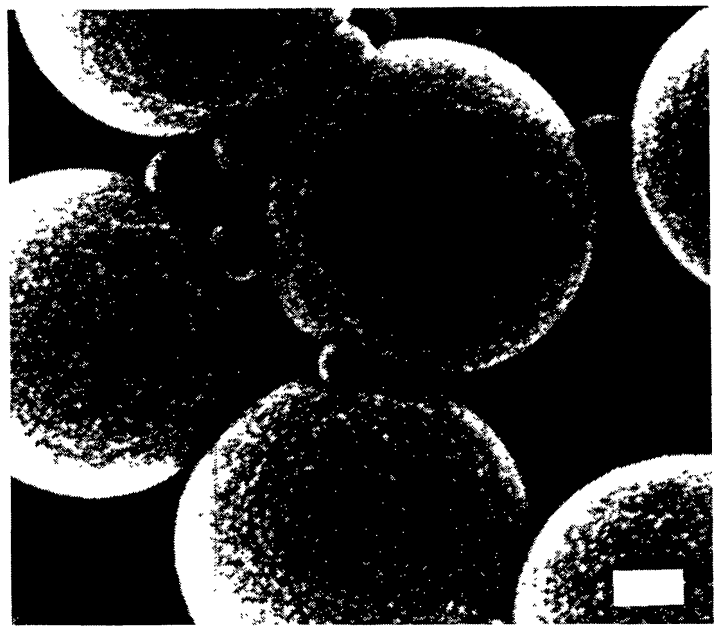

Fig. 2. SEM micrograph; latex spheres 1000, 3000, and 5000 Å in diameter cover a carbon substrate. Forty seconds of sputtering produces a gold artifact surface that retains a few cracks up to 100 Å wide. Islands of gold ranging in size from about 100 to 150 Å cover the surface of the spheres. Width of field is one micron; length of bar is 1000 Å. NASA Photo: S77-25480.

Fig. 3. SEM micrograph; latex spheres 1000, 3000, and 5000 Å in diameter cover a carbon substrate. One hundred eighty seconds of sputtering produces an artifact surface covered by islands of gold that average about 200 Å in diameter. Width of field is one micron; length of bar is 1000 Å. NASA Photo: S77-21556.

could not produce an artifact-free surface using gold, platinum and an Au40:Pd60 alloy were utilized in a similar series of tests following the procedure outlined for Au. Based on these tests the AuPd alloy appears to be the best choice for a coating material. An artifact free and noncharging coating can be produced by sputtering AuPd for 30 seconds, but target to sample distance must be increased to 5 cm. Figure 4 illustrates such an artifact free surface. Note that the magnifications for Figs. 2, 3 and 4 are the same and the resolution for each is the same. The artifact free surface in Fig. 4 represents a much finer grain size of the alloy, and the coating does not obscure nor does it produce surface features.

This new technique was employed in the SEM observation of samples 76015,24,9003 and 76015,28,9004. Microcracks in the anorthite crystal examined in the case of 76015,28,9004 produced some charging and a second coating was required, producing a visible granularity not seen on 76015,24,9003.

RESULTS

There are differences in the microcrater populations and surface characteristics between 76015,28,9004 which was exposed in the plane of the ecliptic and 76015,24,9003 which was exposed perpendicular to the ecliptic plane.

Figure 5 shows the cumulative crater density for 76015,28,9004. The smallest craters observed on this surface are about 200 Å in diameter when measured

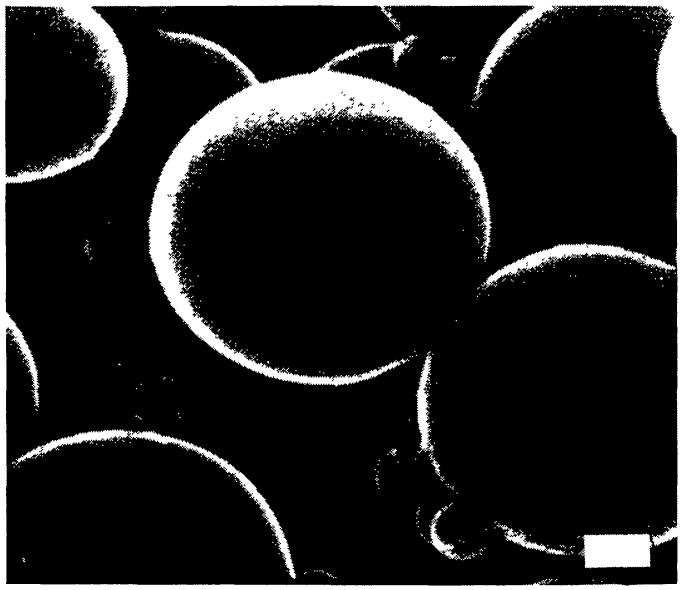

Fig. 4. SEM micrograph; latex spheres 1000, 3000, and 5000 Å in diameter cover a carbon substrate. Thirty seconds of sputtering, Au40Pd60, produces an artifact free surface. Width of field is one micron; length of bar is 1000 Å. NASA Photo: S77-25589.

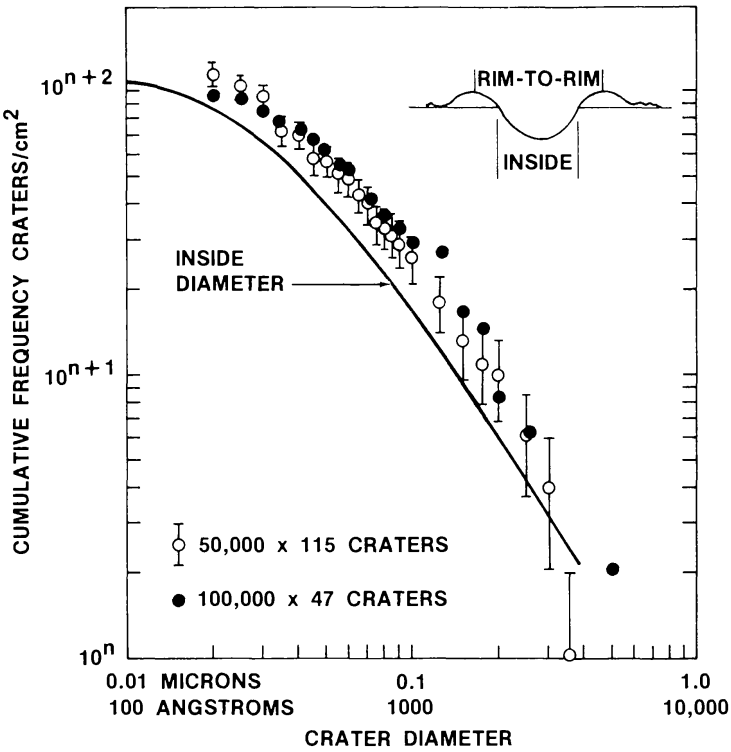

Fig. 5. Cumulative size frequency distribution of microcraters on 76015,28,9004. The inset illustrates the difference between rim-to-rim and inside diameters.

from rim to rim and about 100 Å inside or true diameter (Clanton and Morrison, 1979). The inset of Fig. 5 illustrates the difference between rim to rim and inside diameters. Craters of the smaller diameters are not readily distinguishable in all cases from other surface features, but craters equal to or greater than 300 Å (3 mm at a scale of 100,000x) are readily identifiable.

Figure 6(a–d) illustrates the appearance of craters of various diameters on the surface of 76015,28,9004. The crater shown in Fig. 6b is unusual. The diameter is 0.15 microns rim to rim, and the rim is well developed. Inside the crater is a second crater with a diameter of about 300 Å. The same arrangement was observed in another crater with a diameter of 0.09 microns. In both cases the interior crater lacks a rim. Whether or not the interior craters are impact produced or represent crystal defects revealed by the larger craters is unknown. Figure 6d shows craters with diameters on the order of 300 Å. Rims are visible, but in many cases are not well defined because of a lack of contrast with the background and with the granularity of the surface. A number of craters smaller than those shown in Fig. 6d may be obscured by the background texture.

As can be seen in Fig. 6, the surface of 76015,28,9004, an anorthite crystal, is littered with objects of various shapes and sizes and has a granularity superposed on all other features. The objects, accreta (McDonnell, 1977), range from disks or pancakes (Poupeau *et al.*, 1975; Blanford *et al.*, 1974) to moderately angular fragments. There are very few disks of less than 1000 Å diameter on this surface. Particularly abundant are features with varying degrees of sphericity; most of these are less than 1000 Å diameter and many have diameters of 100 – 200 Å (cf. Fig. 6).

The granularity previously referred to appears to consist of two components; (1) numerous features of several hundred angstroms or less in diameter and not as thick as they are wide, which cover virtually the entire surface, and (2) a graininess resembling a film grain which is the coating artifact mentioned previously.

The craters shown in Fig. 6 appear to be not as crisp compared to the background texture as is generally the case for submicron diameter craters and are not as well defined in general as craters of the same sizes on 76015,24,9003. This characteristic is apparent at a magnification of 100,000x, but not obvious at magnifications of 50,000x.

The cumulative microcrater density for 76015,24,9003 is shown in Fig. 7. It is steeper than the distribution of 76015,28,9004 in the 900 Å to 400 Å diameter interval. Both distributions flatten out for craters of smaller diameters, but are comparable at diameters greater than 900 Å approximately.

Figure 8 shows the surface of 76015,24,9003 with several typical microcraters. The smallest craters observed on this surface are 250 – 300 Å in diameter rim-to-rim with 150 – 200 Å true diameters. The microcraters have the characteristics of those produced by hypervelocity impact (Fig. 8).

The surface of 76015,24,9003, an orthopyroxene crystal, is very different in appearance from 76015,28,9004. Accreta of all types are much less abundant in

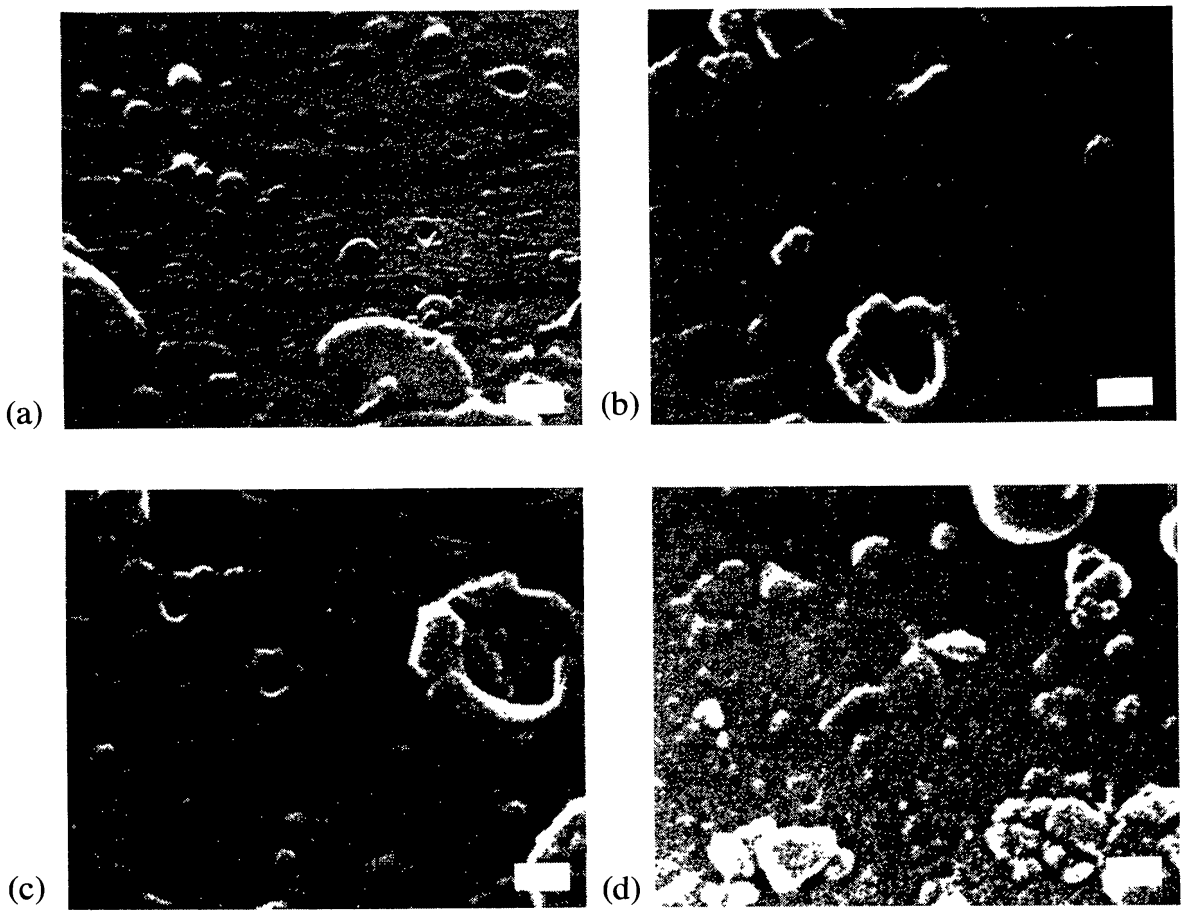

Fig. 6. SEM micrographs of sample 76015,28,9004. Original magnifications were 50,000x (6a) and 100,000x (6b, c, d) (a) Several microcraters and accretionary disks (pancakes) appear in the field of view. Length of bar is 2000 Å, width is 1000 Å. (b) Note the unusual crater-within-crater morphology, bottom center. The "granularity" of the micrograph is an artifact of the stripping and/or coating techniques. (c) Glass and debris partially fill the larger crater. Length of bar is 1000 Å, width is 500 Å. (d) Examples of some of the smallest craters that were measured. Length of bar is 1000 Å, width is 500 Å.

the case of 76015,24,9003. The dominant surface characteristic is an apparent overprinting of forms which vary from worm-like to equidimensional (Fig. 8).

The former are about 100 Å wide and typically have lengths several times their width. These forms are 2 to 3 times smaller on the average than the forms which produce the granularity on 76015,28,9004.

DISCUSSION

Our observations of two lunar sample surfaces at high magnifications represented by the SEM micrographs in Figs. 6 and 8 show microcraters as small as 250 – 300 Å diameter (rim-to-rim) or about 100 – 150 Å true diameter. These microcraters have the attributes of craters produced by hypervelocity impact (cf. Hörz

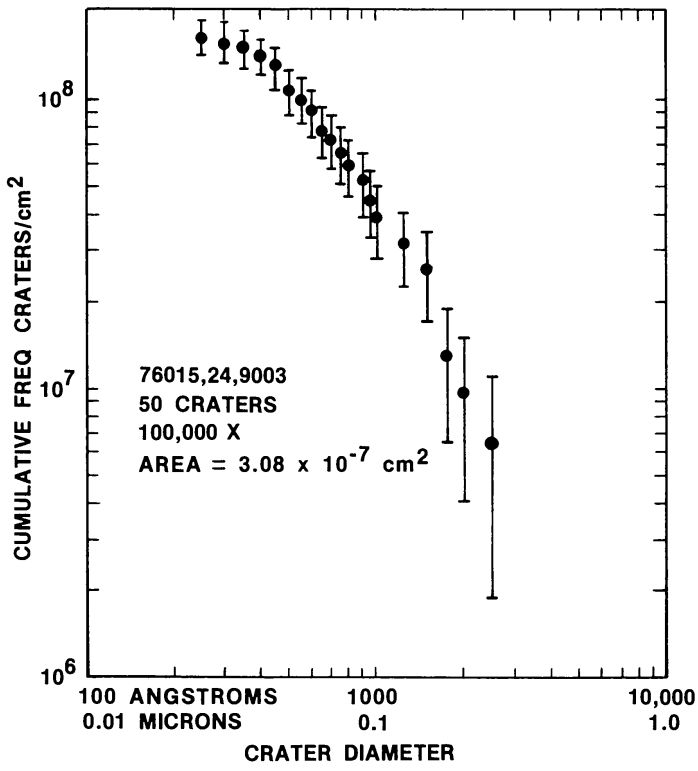

Fig. 7. Cumulative crater frequency for 76015,24,9003. Solid line represents inside diameter. The area measured is shown.

et al., 1975; Neukum *et al.*, 1972), but Nagel *et al.* (1975) have shown that some ejecta from microcraters can reach hypervelocities. A major contribution to the populations we observe from hypervelocity secondaries probably can be ruled out because of the peculiar exposure geometry for 76015,24,9003, which has the steepest distribution. In this case the target surface is situated at the bottom of a narrow cavity. To have hit this target, ejecta from craters produced higher in the cavity would have required trajectories virtually parallel to the cavity walls and negative takeoff angles; an improbable situation. A similar argument cannot be applied to 76015,28,9004 because of the larger volume of the cavity from which it was taken, but 76015,28 has the flatter distribution. We conclude that we are observing microcraters produced by hypervelocity micrometeoroids.

The crater data are plotted as log cumulative density vs. log crater diameter. On these plots, the slope of the microcrater distribution for 76015,24,9003 is ≈ -1.3 (Fig. 7), whereas it is -1 to -1.2 for 76015,28,9004, over the diameter range 1000 Å to 400 Å approximately. In both cases, the distributions flatten for the smallest craters measured. Because the two samples were oriented normal to each other on the lunar surface, it is possible that the different slopes represent different populations of micrometeorites producing craters less than 1000 Å diameter. However, there are some arguments that would qualify this point of view. First, 76015,28,9004 with the shallower slope, has a much higher accreta population and the accreta could selectively obscure craters (compare Figs. 6 and 8).

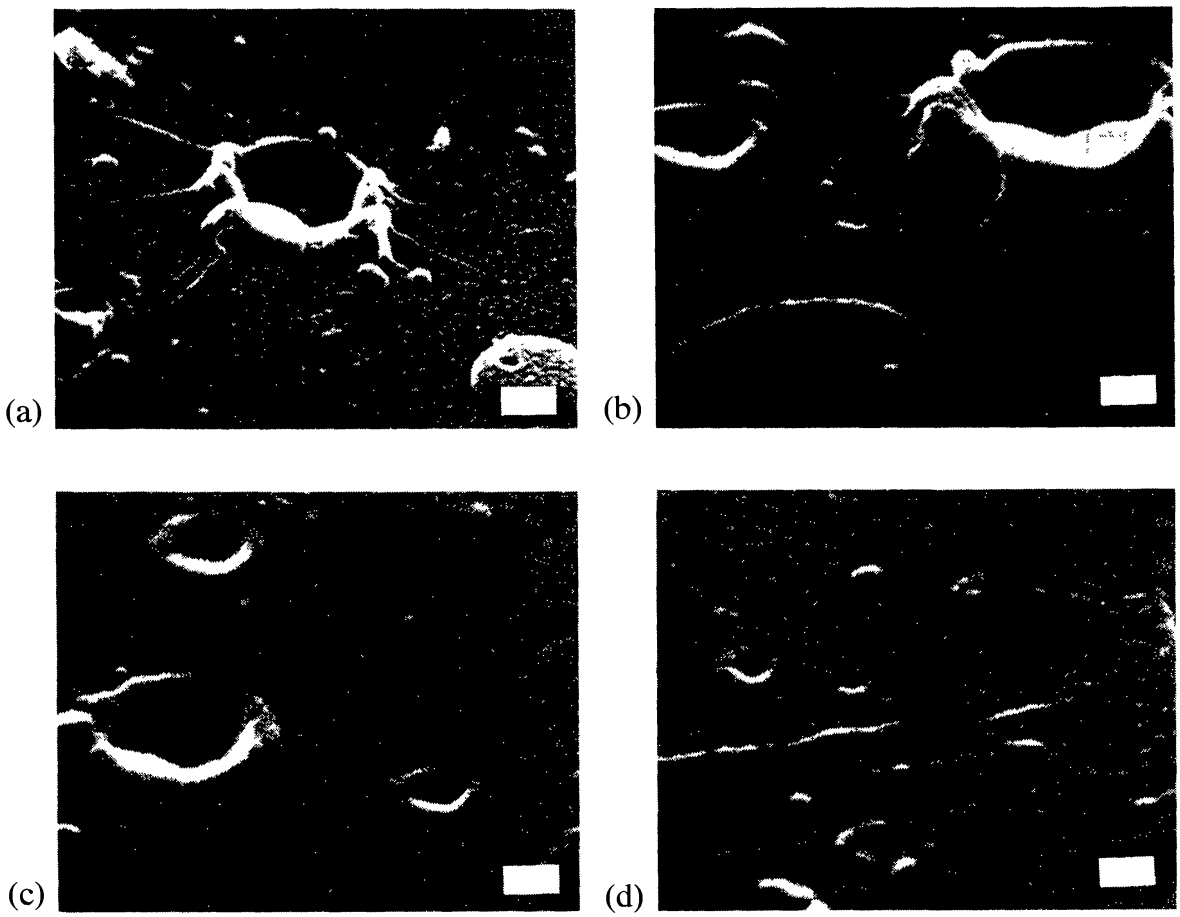

Fig. 8. SEM micrographs of sample 76015,24,9003. Original magnifications were 50,000x (8a) and 100,000x (8b, c, d). (a) Filaments of glass radiate from the largest crater. Note also that the accretionary disk at the lower right has craters. Length of bar is 2000 Å, width is 1000 Å. (b) Filaments of glass have been formed from the rim material of the largest crater. Length of bar is 1000 Å, width is 500 Å. (c) The classic morphology of submicron craters is illustrated in this micrograph. Length of bar is 1000 Å, width is 500 Å. (d) An example of some of the smallest craters observed on the surface of this sample. Length of bar is 1000 Å, width is 500 Å.

Secondly, this sample may have been exposed to the solar wind. Morrison and Zinher (1977) established an upper limit of 0.03 Å per year for solar wind erosion of anorthite under lunar conditions. McDonnell (1977) has determined a value of 0.031 Å ± 30% per year experimentally. With these data plus the exposure geometry, the age of the sample (Morrison and Zinner, 1975), and the rotation of the moon, a removal of 700 – 800 Å from the surface of 76015,28,9004 would be predicted: this would be sufficient to make craters of about 1000 – 1500 Å diameter unrecognizable if exposed for the full term (McDonnell and Carey, 1975), with some flattening of the distribution resulting. We observe no definitive evidence for solar wind erosion, but characteristics such as those described by McDonnell (1977) may be obscured by the patina. The gold-coating stripping technique used for 76015,28,9004 may also have had an effect. A third point

concerns previously established distributions. Poupeau *et al.* (1975), measured crater populations on feldspars from soils 64421 and 60007. Their results, at the highest magnifications used, are shown in Fig. 9 with our two curves, and they are comparable to the steeper distribution for 76015,24,9003. It is unlikely that the exposure geometries of these three samples were identical, suggesting that exposure geometry is not a cause for the differences between 76015,24,9003 and 76015,28,9004. We conclude that the steeper cumulative frequency distributions of 76015,24,9003 and 64421-60007 most accurately reflect the micrometeoroid population producing these small craters.

The distributions for microcraters smaller than 1000 Å diameter join smoothly with the distribution for larger craters from parent samples 76015,28 and 76015,24 as measured by Morrison and Zinner (1975), and shown in Fig. 10. The distribution for craters larger than 1000 Å (0.1 microns) has a slope of –2.5 to –2.6. Below 1000 Å diameter, the distribution has a slope of about –1.3, indicating fewer particles per diameter increment with decreasing diameter. At a diameter of 400 Å the curve begins to flatten, suggesting that relatively few particles producing microcraters of less than 400 Å are present in the micrometeoroid complex.

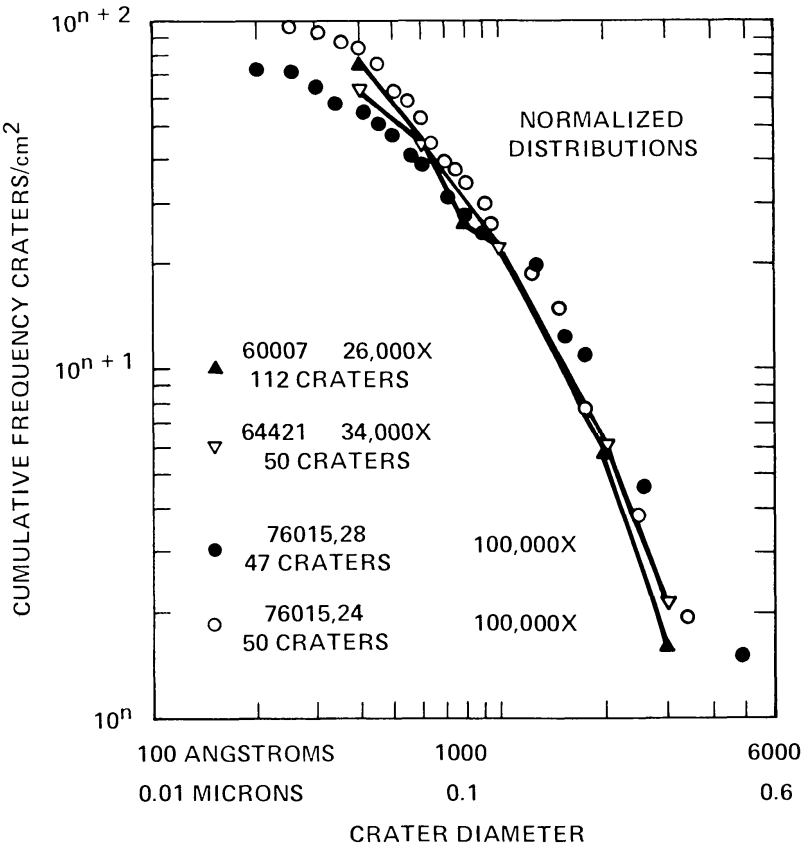

Fig. 9. Comparison of data from 76015 surfaces with craters measured on soil grains (Poupeau *et al.*, 1975). Magnification used in the latter work is shown. 64421 came from a depth of 15 cm and 60007,240 from 2.5 – 3 cm in the lunar regolith.

Some caution should be exercized in the case of the flattening of the curve for microcraters less than 400 Å diameter because of the possibility that smaller craters could be obscured by surface properties as appears to be the case for 76015,28,9004 (Fig. 6) compared to 76015,24,9003 (Fig. 8). The slopes were measured on the latter distribution, but even in this case craters of about 200 Å rim-to-rim could be obscured although larger (e.g., 300 Å) craters appear to be readily recognizable. Because the flattening of the distribution occurs at a diameter of approximately 400 Å, we tentatively conclude that it reflects a property of the micrometeoroid complex.

The conditions of the surfaces of the samples also preclude setting a definite lower size limit for cosmic dust particles because craters of 100 Å diameter or smaller cannot be identified with certainty. The distributions, however, suggest that if such particles exist they are extremely rare.

It is possible to make an estimate of the sizes and masses of the impacting micrometeorites. HEOS data (Hoffman *et al.*, 1975) suggest relative velocities of at least 50 km/sec for micron and submicron diameter micrometeoroids. At these velocities (≈50km/sec), the calibration data of Neukum *et al.* (1972) and

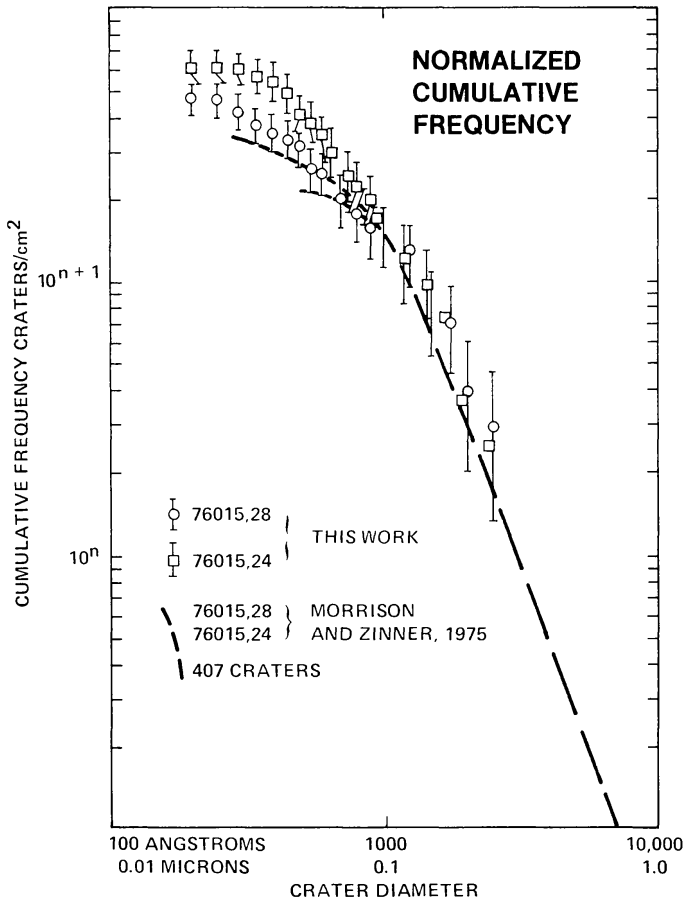

Fig. 10. Crater distributions from 76015,28,9004 and 76015,24,9003 compared with distributions on parent samples ,28 and ,24 measured by Morrison and Zinner (1975) at lesser magnifications.

Nagel *et al.* (1975) indicate a crater diameter to micrometeorite diameter ratio of approximately 4. Consequently the diameters of the particle producing craters of 300 Å diameter (rim-to-rim) or 150 Å true diameter microcraters would be about 40 or 75 Å respectively. Such particles probably are not aggregates and may have densities typical of silicates (2.5 – 3.0 gms per cm^3) or metals such as iron (7.87 gms per cm^3). Masses in these cases would be 1×10^{-20} gms to 5×10^{-19} gms respectively, assuming that the particles are spheres.

Sample 76015,24,9003 was exposed for 4.6×10^5 years (Morrison and Zinner, 1975) at 0.29 steradians (Blanford *et al.*, 1974). The resulting crater production rate is shown in Fig. 11 plotted with the rate for craters up to about 1 mm diameter as determined from 76215 and 12054 (Morrison and Zinner, 1977). The extension of the latter distribution with the new data is justification for the extrapolation of the 12054 data with a –2.5 slope to 0.1 micron diameters which is shown by Morrison and Zinner (1977) and Hartung *et al.* (1978).

All of the microcraters we have observed on both samples are equidimensional with the exception of an elliptical crater with a major axis of 0.15 microns and a minor axis of 0.09 microns, suggesting impact of a rod-like particle.

We have not measured depth to diameter ratios from which inferences concerning particle density may be derived (Nagel *et al.*, 1975). But with the exception of the "doublet" crater shown in Fig. 6B and one other, the craters do not seem to be extraordinarily deep. In fact, particularly in the case of 76015,24,9003 (Fig. 8), they appear to be rather shallow. This assessment is subjective, however, and quantitative measurements are required.

The microcraters we have observed in this work were made by dust particles within the size range of the constituents of the interplanetary dust particles collected by Brownlee *et al.* (1977). According to Brownlee *et al.* (1977), aggregates collected are made of smaller particles which vary from 10 Å to microns, but with typical sizes of ≈1000 Å. Qualitatively, breakup of such aggregates could supply the dust flux producing submicron and smaller craters. It would be interesting to determine if the grain size distribution of the particles collected by Brownlee *et al.* (1977) corresponds to the crater (or particle) size frequency distribution we observe.

CONCLUSIONS

1. Microcraters as small as 100 – 200 Å diameter occur on appropriately exposed lunar surfaces and are produced by cosmic dust particles with diameters of tens of angstroms and masses of 10^{-20} to 5×10^{-19} gms.
2. The cumulative crater frequency distribution curve shows a relative decrease in the density of craters less than 1000 Å diameter (and associated dust particles) compared to larger craters.
3. The distribution, crater production rates, and micrometeoroid flux derived fit the earlier results of Morrison and Zinner (1977) for larger craters and micrometeoroids.

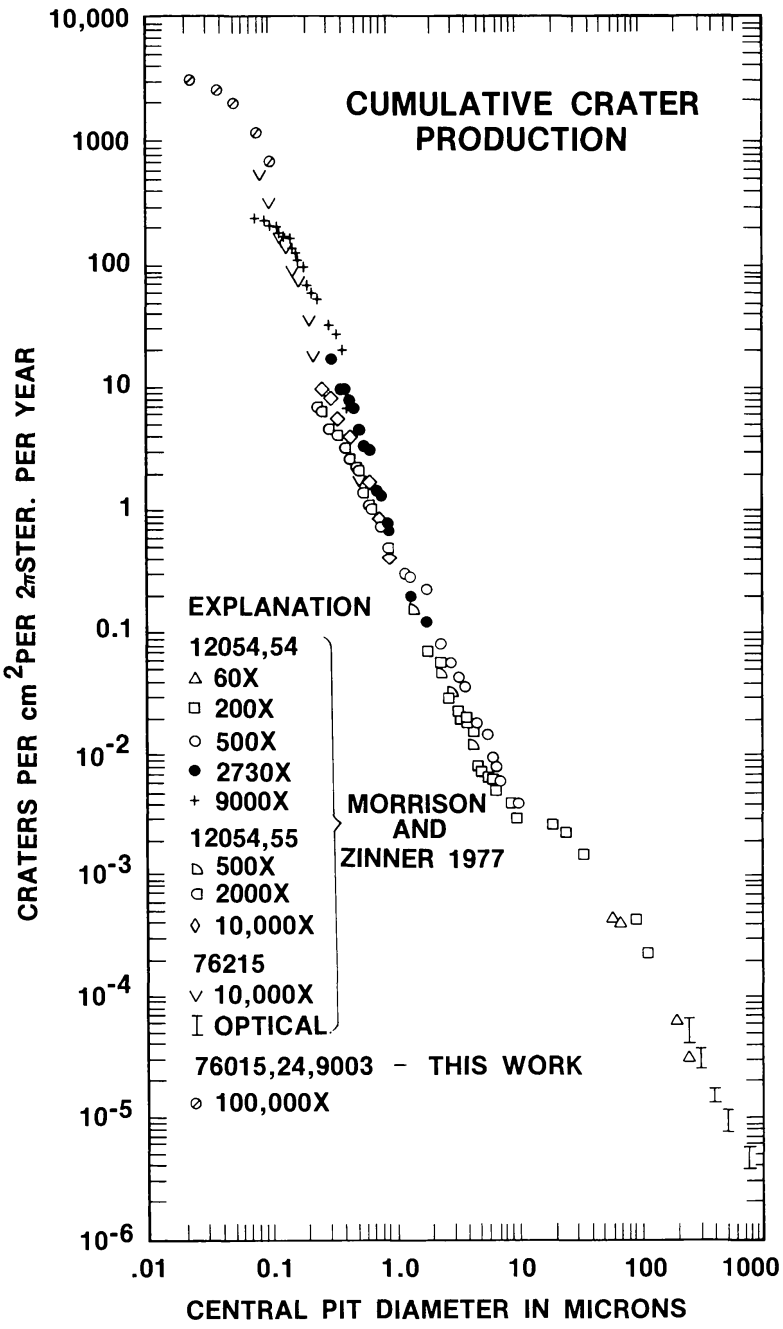

Fig. 11. The production rate of microcraters over the diameter interval 0.01 to 1000 microns from this work and the data of Morrison and Zinner (1977). Not all of the data of the latter is plotted.

4. For craters between 0.1 and about 5 – 7 microns, diameter and slope of the crater distribution curve is about –2.5 on a log-log plot. Between 400 Å (0.04 microns) and 1000 Å (0.1 microns), the slope is approximately –1.3. The distribution flattens to a slope of near 0 for crater diameters less than 400 Å.
5. The microcrater distributions we measured on 76015 samples exposed in

the last 500,000 years are comparable to the microcrater distributions on soil grains (Poupeau *et al.*, 1975) exposed at some time in the past, suggesting continuity of the processes involved.

6. No lower limit in microcrater size can be definitely stated, but particles of $\approx 10^{-20}$ gms producing microcraters of $\approx 100 - 200$ Å must be extremely rare.
7. The microcraters observed could have been produced by grains making up the particles collected by Brownlee *et al.* (1977).

Acknowledgments—We wish to acknowledge conversations with S. Rajan who pointed out to us some aspects of the physics affecting small dust particles in the interplanetary medium. Reviews by J. Rajan, E. Zinner and an anonymous reviewer improved the manuscript. We acknowledge E. Stockton for manuscript preparation.

REFERENCES

Blanford G. E., Fruland R. M., McKay D. S., and Morrison D. A. (1974) Lunar surface phenomena: Solar flare track gradients, microcraters and accretionary particles. *Proc. Lunar Sci. Conf. 5th,* p. 2501–2526.

Brownlee D. E., Tomandl D. A., and Olszewski E. (1977) Interplanetary dust: A new source of extraterrestrial materials for laboratory studies. *Proc. Lunar Sci. Conf. 8th,* p. 149–160.

Clanton U. S. and Morrison D. A. (1979) Hypervelocity impact craters less than 1000 Å diameter (abstract). In *Lunar and Planetary Science X,* p. 212–214. Lunar and Planetary Institute, Houston.

Hartung J. B., Hauser E. E., Hörz F., Morrison D. A., Schonfeld E., Zook H. A., Mandeville J. C., McDonnell J. A. M., Schaal R. B., and Zinner E. (1978) Lunar surface processes: Report of the 12054 consortium. *Proc. Lunar and Planet. Sci. Conf. 9th,* p. 2507–2537.

Hoffman H. J., Fechtig H., Grün E., and Kissel J. (1975) First results of the micrometeoroid experiment S-215 on the HEOS 2 satellite. *Planet. Space Sci.* **23,** p. 215–224.

Hörz F., Brownlee D. E., Fechtig H., Hartung J. B., Morrison D. A., Neukum G., Schneider E., Vedder J. F., and Gault D. E. (1975) Lunar microcraters: Implications for the micrometeoroid complex. *Planet. Space Sci.* **23,** p. 151–172.

McDonnell J. A. M. (1977) Accretionary particle studies on Apollo 12054,58: In-situ lunar surface microparticle flux rate and solar wind sputter rate defined. *Proc. Lunar Sci. Conf 8th,* p. 3835–3857.

McDonnell J. A. M. and Carey W. C. (1975) Solar wind sputter erosion of microcrater populations on the lunar surface. *Proc. Lunar Science Conf. 6th,* p. 3391–3402.

Morrison D. A. and Zinner E. (1975) Studies of solar flares and impact craters in partially protected crystals. *Proc. Lunar Sci. Conf. 6th,* p. 3373–3390.

Morrison D. A. and Zinner E. (1977) 12054 and 76215: New measurements of interplanetary dust and solar flare fluxes. *Proc. Lunar Sci. Conf. 8th,* p. 841–863.

Nagel K., Neukum G., Eichhorn G., Fechtig H., Müller O., and Schneider E. (1975) Dependencies of microcrater formation on impact parameters. *Proc. Lunar Sci. Conf. 6th,* p. 3417–3432.

Neukum G., Schneider E., Mehl A., Storzer D., Wagner G. A., Fechtig H., and Bloch M. R. (1972) Lunar craters and exposure ages derived from crater statistics and solar flare tracks. *Proc. Lunar Sci. Conf. 3rd,* p. 2793–2810.

Poupeau G., Walker R. M., Zinner E., and Morrison D. A. (1975) Surface exposure history of individual crystals in the lunar regolith. *Proc. Lunar Sci. Conf. 6th,* p. 3433–3448.